JOURNAL OF GUIDANCE, CONTROL, AND DYNAMICS
Vol. 33, No. 1, January–February 2010

Desensitizing the Minimum-Fuel Powered Descent for Mars Pinpoint Landing

Haijun Shen,* Hans Seywald,† and Richard W. Powell‡
Analytical Mechanics Associates, Inc., Hampton, Virginia 23666

DOI: 10.2514/1.44649

This paper aims at reducing the sensitivity of the minimum-fuel powered descent trajectory on Mars in the presence of uncertainties and perturbations, using the desensitized optimal control methodology. The lander is modeled as a point mass in a uniform gravitational field, and the engine throttle is considered the control variable, which is bounded between two nonzero settings. Unlike the conventional practice of designing separately the nominal trajectory and a feedback tracking controller, desensitized optimal control strategy incorporates the two designs in synergy, delivering a superior performance. Sensitivities of the final position and velocity with respect to perturbed states at all times are derived and augmented onto the minimum-fuel performance index through penalty factors. The linear quadratic regulator technique is used to design the feedback control gains. To reduce the likelihood of the closed-loop throttle exceeding the prescribed bounds, a multiplicative factor is applied to the feedback gains. This reshapes the nominal trajectory from the well-known maximum–minimum–maximum structure in that the nominal throttle is encouraged to stay away from the prescribed bounds, leaving room for the feedback control. Monte Carlo simulations show that the occurrence of out-of-bound closed-loop throttles is significantly reduced, leading to improved landing precision.

Introduction

THE landing accuracy on the surface of Mars has progressed steadily over the last four decades, [1–3] from about 200 km of target for the Vikings to 150 km for the Mars Pathfinder to 35 km for the Mars Exploration Rovers. In these missions, the landing accuracy is not critical to their success because they are mostly exploratory in nature, and the spacecraft are only required to land safely in the general vicinity of the targeted landing sites. Mars Science Laboratory (MSL) is the next in line to be launched. Despite being exploratory as well, it will have a much improved landing accuracy, with a delivery of within 10 km of the target. The next generation of Mars missions such as the sample return and human exploration missions will require Mars probes to perform tasks at specific points of interest on the Martian surface. Thus, the performance of pinpoint landings (defined as landing within 100 m of the target) [4] will be of utter importance. Much of the work in improving the landing accuracy has been focused on advancing the navigation technologies to obtain more precise measurements of the position and velocity of the spacecraft [5–7]. In addition, the actively guided entry through modulating the lift vector (on MSL, for example) [2,8–10], as well as the smart-chute technique [11,12] also play significant roles in improving the landing accuracy.

This study focuses on the powered descent stage, which commences when the entry vehicle is decelerated to about 55–90 m/s on the parachute, typically at 3–5 km altitude and roughly a few kilometers from the prescribed landing target horizontally. At this moment, the parachute and the heat shield are released. A set of rocket engines are used to guide the lander to the target, and the throttle of the engines as well as the thrusting direction are considered as the controls. For missions in which precision landing is not important, gravity turn trajectories are typically chosen to land the spacecraft safely at the landing site. Very limited studies have been performed on the powered descent guidance with the pinpoint landing requirements. Reference [13] proposes to use polynomials of time to describe the desired position, velocity, and acceleration profiles, and the lander is commanded to follow the prescribed trajectory. Although this method is autonomous in nature, no fuel optimization is considered. Two studies have been devoted to finding the minimum-fuel descent trajectories. Reference [14] shows that the minimum-fuel throttle profile is of maximum–minimum–maximum structure. Because the minimum engine throttle cannot be zero once the engine is turned on, [15] points out that the optimization problem is nonconvex. Consequently, a convex model is proposed, and it is proven that the optimal solution to the convexified model is precisely that to the original nonconvex problem.

However, the maximum–minimum–maximum throttle profile is an open-loop strategy. In the presence of perturbations, the open-loop strategy leads to great errors at the final time. Often in practice, when perturbations are encountered, a feedback control law is devised to guide the lander to the vicinity of the planned target via a trajectory that is in the neighborhood of the nominal trajectory [16]. In conventional practice, the designs of the feedback law and the nominal trajectory are conducted completely separately; that is, the design of the nominal trajectory does not take into consideration what feedback law may be used later. Thus, the performance of the feedback control law is often not guaranteed. One example that embodies the drawbacks of such design process has to do with the nominal maximum–minimum–maximum throttle profile. Since the open-loop throttle rides on the bounds in the nominal solution, the closed-loop throttle is highly likely to exceed the bounds, and thus the out-of-bound closed-loop throttle cannot be executed fully. The regular exercise of scaling the out-of-bound control can lead to large errors in practice. Resolving these issues will be a focal point of this paper.

A more appropriate optimal control design approach is to design the nominal control and the feedback law in synergy and to have both aspects of the design work together to achieve a better performance. That is precisely the virtue of the desensitized optimal control (DOC) strategy [17]. In a nutshell, DOC tries to reduce the sensitivity of a physical quantity with respect to uncertainties and perturbations along the trajectory, in addition to optimizing the original performance index. (In the context of the powered descent problem, the final position and velocity of the lander can be examples of such physical quantities.) DOC does this by incorporating the feedback

Presented at the 19th AAS/AIAA Spaceflight Mechanics Meeting, Savannah, GA, 8–12 February 2009; received 30 March 2009; revision received 23 August 2009; accepted for publication 27 August 2009. Copyright © 2009 by the American Institute of Aeronautics and Astronautics, Inc. All rights reserved. Copies of this paper may be made for personal or internal use, on condition that the copier pay the $10.00 per-copy fee to the Copyright Clearance Center, Inc., 222 Rosewood Drive, Danvers, MA 01923; include the code 0731-5090/10 and $10.00 in correspondence with the CCC.

*Senior Project Engineer, 303 Butler Farm Road, Suite 104A; shen@ama-inc.com. Member AIAA.
†Staff Scientist; seywald@ama-inc.com. Member AIAA.
‡Senior Technical Advisor; r.powell@ama-inc.com. Associate Fellow AIAA.

law design into the nominal control optimization. Thus, the nominal control and the feedback law are obtained in one optimization run. As is always the case, the goal of the sensitivity reduction and the original performance index are two conflicting objectives. As a result, both objectives compromise to each other during the optimization process. Therefore, the nominal trajectory is reshaped from its original form without the sensitivity consideration. One factor that affects the extent of the reshaping is the design of the feedback law. In this paper, the linear quadratic regulator (LQR) technique [16] is used to design the feedback law to minimize the final position and velocity deviation from the target as well as the amount of control effort.

To specifically address the issue of the closed-loop control exceeding the prescribed bounds, a user-defined multiplicative factor is applied to the feedback gain to discourage the nominal control from approaching the bounds too closely. The multiplicative factor becomes zero as the nominal control rides the bounds and thus effectively eliminates the sensitivity reduction effect of the feedback law. It also monotonically increases with the distance between the nominal control and the bounds, partially resuming the function of the feedback law. Therefore, in order for the sensitivity of the final position and velocity to be reduced through the feedback mechanism, the nominal control profile has to stay away from the prescribed bounds. That also explains the reshaping of the nominal trajectory.

Achieving robustness of the system performance in the presence of perturbations is not a new concept [18–20]. However, most of the methods are not readily applicable to the minimum-fuel powered descent problem, due to its nonlinear nature. The concept of the chance-constrained programming [19,20] can potentially be used to design controllers tracking the maximum–minimum–maximum nominal control, in that it can enforce the constraint on the probability of the control bound violation given input disturbances with known probability distributions. However, when the nominal control is reshaped in DOC to no longer be maximum–minimum–maximum and is not known a priori, it is not clear how control bound violations can be measured.

This paper is organized as follows. First, the formulation of the minimum-fuel powered descent problem is described. Then a brief overview of the sensitivity analysis is presented, and the sensitivity of the final position and velocity with respect to state perturbations are derived and augmented into the minimum-fuel powered descent problem. The method of treating control bounds is presented next, followed by the design of the feedback laws. Simulation results and the conclusions are presented in the end.

Minimum-Fuel Powered Descent Problem

The powered descent phase of a Mars landing trajectory typically starts when the parachute and heat shield are jettisoned (the hand-off), and from then on, thrusters are used to guide the lander to a safe landing site. During the powered descent phase, the lander is typically traveling below an altitude of 5 km and with a speed less than 95 m/s. Therefore, in a typical problem formulation [14,15], a uniform gravitational field is used, and the aerodynamic forces and the rotation of the planet are neglected. In addition, the lander is modeled as a point mass in this study, and the much more complex problem of coupled translational and attitude guidance is beyond the scope of this paper.

A surface-fixed coordinate system $O\hat{x}\,\hat{y}\,\hat{h}$ is defined to describe the position and velocity of the lander. The origin is anchored at the planned landing point, the $\hat{x}$ and $\hat{y}$ axes span the horizontal plane, and the $\hat{h}$ axis points upward. Let v_x, v_y, and v_h denote the velocities along the three axes, and let m denote the mass of the lander. Then the state vector is completely defined as $\mathbf{x} = [x, y, z, v_x, v_y, v_z, m]^T$. Let g denote the gravitational acceleration on the surface of Mars, and let g_0 denote that at the sea level on Earth. Let there be n identical thrusters with specific impulse I_{sp}. Each thruster supplies a maximum thrust T and is throttled at the same level, which leads to all the thrusters producing the same thrust at any time. The thrusters are mounted such that they are canted at an angle ϕ from the net thrust direction. Thus, the net thrust is given by $n \cdot T \cdot \cos\phi$.

The translational motion of the lander is controlled via modulating the throttle of the thrusters and the direction of the net thrust vector. Let $\mathbf{u}$ be the vector that points in the direction of the net thrust and has a magnitude of the thruster throttle u. Let u_x, u_y, and u_h be the three components of $\mathbf{u}$ along the $\hat{x}$, $\hat{y}$, and $\hat{h}$ axes. Then $\mathbf{u} = [u_x, u_y, u_h]^T$ can serve as the control vector. With the above definitions, the differential equations of the translational motion can be written as

$$\dot{x} = v_x, \qquad \dot{y} = v_y, \qquad \dot{h} = v_h, \qquad \dot{v}_x = \frac{u_x \cdot n \cdot T \cdot \cos\phi}{m}$$
$$\dot{v}_y = \frac{u_y \cdot n \cdot T \cdot \cos\phi}{m}, \qquad \dot{v}_h = -g + \frac{u_h \cdot n \cdot T \cdot \cos\phi}{m}$$
$$\dot{m} = -\frac{u \cdot n \cdot T}{I_{\text{sp}} \cdot g_0} \tag{1}$$

Once the thrusters are switched on, they remain on throughout the descent. Thus, the engine throttle is bounded between two nonzero settings; i.e.,

$$0 < u_{\min} \le u = \sqrt{u_x^2 + u_y^2 + u_h^2} \le u_{\max} \tag{2}$$

The position and velocity at both ends of the powered descent trajectory are specified. The initial condition, denoted by $\mathbf{x}_0$, is given at the hand-off, and the lander at the end of the descent is at rest at the planned landing point. The assumption of zero final position and velocity vectors is only representative of practice, because in reality, the final position would be a few tens of meters above the surface, and the vehicle would have a nonzero downward vertical velocity to allow for the final touchdown. During the powered descent, the spacecraft obviously cannot travel below the planet surface, which leads to the following state constraint:

$$h(t) > 0, \quad \forall\ t \tag{3}$$

There are many other state constraints in reality, such as the glide slope constraint considered in [15], which constrains the slope at which the lander approaches the landing site. However, the inclusion of these constraints does not change the structure of the solution, and thus these constraints are not considered. The final time is free. The objective of the optimal control is to guide the lander from the initial conditions to the final conditions with the minimum amount of fuel consumption; that is, the minimum-fuel powered descent problem can be written as

$$\text{problem no-DOC: } \mathcal{J}_0 = \min_{u_x, u_y, u_h} -m(t_f)$$
$$\text{subject to Eqs. (1), (2), and (3)}; \qquad t_f \text{ is free};$$
$$\mathbf{x}(t_0) = \mathbf{x}_0, \qquad \mathbf{r}(t_f) = 0, \qquad \mathbf{v}(t_f) = 0 \tag{4}$$

where $\mathbf{r}(t)$ and $\mathbf{v}(t)$ denote the position and velocity vectors at time t. References [14,15] provide extensive analyses on the characteristics of this optimization problem. Therein, it is shown that the minimum-fuel throttle profile is of maximum–minimum–maximum structure. In the sequel, the optimal solution to this problem will be termed nominal no-DOC solution.

DOC and Sensitivity Penalties

In reality, the trajectory flown for an actual mission is almost never the nominal trajectory, as there are always uncertainties and perturbations along the trajectory which divert the spacecraft off the nominal path. For a pinpoint landing, excessive deviation from the nominal target may in effect cause the mission to fail. The DOC methodology is designed to reduce the sensitivity of a given physical quantity with respect to the uncertainties and perturbations and, at the same time, to optimize the original objective [17]. Within the context of this paper, this physical quantity can simply be the final position and velocity. It is assumed that once perturbations are encountered, the trajectory continues in the neighborhood of the nominal path through a linear feedback tracking control law. Conventionally, the

feedback controller is designed after the nominal trajectory is obtained. The philosophical difference in the DOC methodology is that the objective of using a feedback law to attenuate uncertainties and perturbations is consolidated into the original optimization problem. As a result, the design of the feedback law has influence on the outcome of the nominal trajectory, and vice versa. That is, the burden of perturbation attenuation is not solely placed on the feedback law design. Instead, the nominal trajectory also takes on a new form that facilitates this objective. An extensive treatment of the sensitivity analysis and the DOC methodology is given in [17]. Here, only a brief overview is provided.

Let $f(\mathbf{x}, \mathbf{u}, t)$ denote the vector of the right-hand side of Eq. (1). Let $X(t|t_0, \mathbf{x}_0)$ denote the solution of Eq. (1) subject to the initial condition $\mathbf{x}(t_0) = \mathbf{x}_0$, and let $\mathcal{S}(t|t_0, \mathbf{x}_0)$ be the matrix defined by

$$\dot{\mathcal{S}}(t|t_0, \mathbf{x}_0) = \left[\frac{\partial f}{\partial \mathbf{x}} + \frac{\partial f}{\partial \mathbf{u}} \cdot \frac{\partial \mathbf{u}}{\partial \mathbf{x}}\right]\Bigg|_{\mathbf{x}=X(t|t_0,\mathbf{x}_0)} \cdot \mathcal{S}(t|t_0, \mathbf{x}_0) \tag{5}$$

and $\mathcal{S}(t_0|t_0, \mathbf{x}_0)$ is the identity matrix I. The important property of the matrix $\mathcal{S}(t|t_0, \mathbf{x}_0)$ is that it represents the sensitivity of the state $X(t|t_0, \mathbf{x}_0)$ with respect to perturbations in the initial state $\mathbf{x}_0$; that is,

$$\mathcal{S}(t|t_0, \mathbf{x}_0) = \frac{\partial X(t|t_0, \mathbf{x}_0)}{\partial \mathbf{x}_0}$$

Thus, Eq. (5) represents a first-order approximation for the variations of state dynamics at time t due to variations at the initial states. In addition, for any $t_1 \in [t_0, t_f]$, the inverse of $\mathcal{S}(t|t_1, X(t_1|t_0, \mathbf{x}_0))$ represents the sensitivity of the solution X at t_1 with respect to changes in the current state $\mathbf{x}(t)$. In the sequel, without causing ambiguity, a simpler notation $\mathcal{S}(t_2, t_1)$ will be used to denote the sensitivity matrix of the state $X(t_2|t_0, \mathbf{x}_0)$ with respect to perturbations in the state $X(t_1|t_0, \mathbf{x}_0)$, and the following property holds:

$$\mathcal{S}(t_2, t_1) = \mathcal{S}(t_2, t_0) \cdot \mathcal{S}(t_1, t_0)^{-1} \tag{6}$$

Let $\mathbf{u}^*(t)$ and $\mathbf{x}^*(t)$ denote the control and state vectors of the nominal trajectory at t. Clearly, when perturbations are encountered, the trajectory will deviate from $\mathbf{u}^*(t)$ and $\mathbf{x}^*(t)$. It can possibly be one of a whole field of trajectories in the neighborhood of the nominal solution. In the DOC framework, it is assumed that the perturbed trajectories are within the bunch reachable by a linear feedback law; that is,

$$\mathbf{u}(t) = \mathbf{u}^*(t) + K(t) \cdot (\mathbf{x}(t) - \mathbf{x}^*(t)) \tag{7}$$

where $K(t)$ denote the feedback gain matrix. $K(t)$ can be either prescribed a priori or can be determined optimally in parallel to the calculation of the optimal nominal trajectory. Substitute Eq. (7) into Eq. (5), and the sensitivity matrix differential equation becomes

$$\dot{\mathcal{S}}(t, t_0) = \left(\frac{\partial f}{\partial \mathbf{x}} + \frac{\partial f}{\partial \mathbf{u}} \cdot K(t)\right) \cdot \mathcal{S}(t, t_0) \tag{8}$$

Once a physical quantity is identified for which the sensitivity with respect to perturbations is to be reduced, one can derive the sensitivity using the above properties of the sensitivity matrix. A form of penalty to the sensitivity is then added to the original performance index, resulting in a consolidated optimal control problem that includes the original dynamics, the sensitivity dynamics, and the new performance index. This concept becomes clearer in the remainder of this section as the desensitization of the powered descent trajectory is formulated.

In the powered descent problem, it is the sensitivity of the final position and velocity with respect to perturbations that needs to be minimized. To this end, Let $\xi(\mathbf{x}(t_f), t_f)$ denote the vector containing the position and velocity components of the lander at t_f; that is,

$$\xi(\mathbf{x}(t_f), t_f) = [x(t_f), y(t_f), h(t_f), v_x(t_f), v_y(t_f), v_h(t_f)]^T$$

Then the sensitivity of $\xi(\mathbf{x}(t_f), t_f)$ with respect to state perturbations at any time t can be written as

$$\frac{\partial \xi(\mathbf{x}(t_f), t_f)}{\partial \mathbf{x}(t)} = \frac{\partial \xi(\mathbf{x}(t_f), t_f)}{\partial \mathbf{x}(t_f)} \cdot \mathcal{S}(t_f, t) \tag{9}$$

Since the state vector $\mathbf{x}$ is of length 7 in this study, $\mathcal{S}(\cdot, \cdot)$ is a 7×7 matrix. Thus, $\partial \xi(\mathbf{x}(t_f), t_f)/\partial \mathbf{x}(t)$ contains the first six rows of matrix $\mathcal{S}(t_f, t) = \mathcal{S}(t_f, t_0) \cdot \mathcal{S}(t, t_0)^{-1}$. Apparently, each element of these rows needs to be minimized at all times. This objective is reflected by the choice of the following performance index:

$$\min \mathcal{J}_1 = \int_{t_0}^{t_f} \sum_{i=1}^{6} \left\{ c_i \cdot \sqrt{\sum_{j=1}^{7} \mathcal{S}_{i,j}(t_f, t)^2} \right\} \mathrm{d}t, \qquad c_i \geq 0 \tag{10}$$

where $\mathcal{S}_{i,j}(t_f, t)$ is the (i, j) element of the matrix $\mathcal{S}(t_f, t)$. Clearly, weights c_1 to c_3 leverage the significance of the final position dispersions to the success of the mission, and c_4 to c_6 leverage that of the final velocity dispersions. For the powered descent problem, much larger horizontal dispersions can be tolerated than vertical dispersions, because negative vertical dispersions may cause the spacecraft to crash into the planet surface. Therefore, one can set c_3 greater than c_1 and c_2 to place more weight on reducing the final altitude dispersion.

The addition of the new performance index turns the minimum-fuel powered descent problem (problem no-DOC) into a multiobjective optimization problem with two conflicting objectives: that is, to minimize $\mathcal{J}_0$ and $\mathcal{J}_1$ at the same time. This paper uses the penalty factor method to consolidate the two objectives, resulting in the following performance index:

$$\mathcal{J} = \min_{u_x, u_y, u_h} (\mathcal{J}_0 + c_0 \cdot \mathcal{J}_1) \tag{11}$$

where $c_0 \geq 0$ denotes the penalty factor on the sensitivity performance index.

With the consolidated performance index, the minimum-fuel powered descent trajectory optimization problem with the sensitivity penalty can be written as follows:

$$\begin{aligned} &\text{problem DOC}_1\text{: } \min_{u_x, u_y, u_h} \mathcal{J} = \mathcal{J}_0 + c_0 \cdot \mathcal{J}_1 \\ &\text{subject to Eqs. (1), (8), (2), and (3);} \qquad t_f \text{ is free;} \\ &\mathbf{x}(t_0) = \mathbf{x}_0, \quad \mathbf{r}(t_f) = 0, \quad \mathbf{v}(t_f) = 0, \quad \mathcal{S}(t_0, t_0) = I_{7\times 7} \end{aligned} \tag{12}$$

Problem DOC_1 differs from problem no-DOC in the former's inclusion of the sensitivity dynamics, the additional performance index, and the initial condition of the sensitivity matrix. Clearly, the solution to problem DOC_1 is the result of compromise between the two objectives of minimizing $\mathcal{J}_0$ and $\mathcal{J}_1$. Thus, the optimal trajectory for problem DOC_1 is different from that of problem no-DOC (*the* fuel-optimal solution); that is, the optimal trajectory is reshaped to one with reduced sensitivity to state perturbations.

Note that c_0, along with the feedback gain matrix $K(t)$, affects how the optimal trajectory is reshaped. When $c_0 = 0$, all related to the sensitivity minimization becomes irrelevant, and problem DOC_1 becomes identical to problem no-DOC. As c_0 increases, more and more emphasis is placed upon minimizing the sensitivity performance index. Consequently, the optimal trajectories become less and less sensitive to uncertainties and perturbations. Naturally, although the solution to problem DOC_1 is less sensitive than the no-DOC solution, it also incurs more fuel consumption. A proper tradeoff can be obtained through picking an appropriate value for c_0. On the other hand, as it has been shown by examples before [17,21] and will be shown later in this paper that a great deal of sensitivity reduction can be achieved with a relatively small increase in fuel consumption.

Treating the Control Constraints

It has been shown in [14,15] that the optimal throttle profile for problem no-DOC is of maximum–minimum–maximum structure. This can be explained by the fact that the control vector $\mathbf{u}$ appears linearly in Eq. (1) but does not explicitly show up in the objective function $\mathcal{J}_0$. An examination of problem DOC_1 reveals that it possesses the same properties. Thus, the optimal throttle for problem DOC_1 is of maximum–minimum–maximum profile as well. However, the maximum–minimum–maximum throttle profile brings challenges to the control implementation. If the nominal control rides on the prescribed bounds, it is highly likely that the closed-loop feedback control would exceed the bounds. Tracking errors are guaranteed when implementing an out-of-bound control, due to lack of enough control authority. This section presents a method that alleviates this problem.

Intuitively, the closer the nominal control is to the bounds, the more likely the closed-loop control is to exceed the bounds. Since the magnitude of the feedback control is proportional to the control gains, it is only natural to choose gains that adapt to the nominal control in a way that the gains gradually decrease as the nominal control approaches the prescribed bounds and become zero when the nominal control rides on the bounds. One way to achieve this is to modulate the gains through a multiplicative factor $\eta(t)$, which possesses this very characteristic. That is, the feedback law in Eq. (7) becomes

$$\mathbf{u}(t) = \mathbf{u}^*(t) + \eta(t) \cdot K(t) \cdot (\mathbf{x}(t) - \mathbf{x}^*(t)) \tag{13}$$

The following $\eta(t)$ is used in the study, which has been tested to work well for most problems:

$$\eta(t) = \frac{4 \cdot (u^*(t) - u_{\min}) \cdot (u_{\max} - u^*(t))}{(u_{\max} - u_{\min})^2} \tag{14}$$

It can be seen that at any time t, $\eta(t)$ is a quadratic function of the nominal control magnitude within its bounds. The maximum $\eta(t) = 1$ when the nominal control is halfway between the bounds (furthest away from the bounds), and the minimum $\eta(t) = 0$ when the nominal control reaches either bound. With the new feedback control given in Eq. (13), the dynamics for the sensitivity matrix are changed accordingly as follows:

$$\dot{\mathcal{S}}(t, t_0) = \left(\frac{\partial f}{\partial \mathbf{x}} + \frac{\partial f}{\partial \mathbf{u}} \cdot \eta(t) \cdot K(t) \right) \cdot \mathcal{S}(t, t_0) \tag{15}$$

Thus, problem DOC_1 in Eq. (12) is changed to

$$\text{problem DOC: } \min_{u_x, u_y, u_h} \mathcal{J} = \mathcal{J}_0 + c_0 \cdot \mathcal{J}_1$$

$$\text{subject to Eqs. (1), (14), (15), (2), and (3); } \quad t_f \text{ is free;}$$

$$\mathbf{x}(t_0) = \mathbf{x}_0, \quad \mathbf{r}(t_f) = 0, \quad \mathbf{v}(t_f) = 0, \quad \mathcal{S}(t_0, t_0) = I_{7\times 7} \tag{16}$$

The solution to this problem will be referred to as the DOC solution in the sequel.

The optimal control profile for the problem DOC is no longer maximum–minimum–maximum. This assertion can be explained by the fact that the control variables do not appear linearly in the problem DOC, as evident in Eqs. (14) and (15). Furthermore, note that when the nominal control is equal to either of the bounds, the effect of the feedback control vanishes because $\eta(t) = 0$ in Eq. (13). Thus, the nominal control is encouraged to stay away from the bounds whenever a leverage can be gained toward the reduction of sensitivity through the feedback law. Clearly, the maximum leverage is obtained when the nominal control is halfway between the bounds, because the fully intended magnitude of the feedback gain is applied. However, the downside of this solution is that it may incur excessive amount of additional fuel consumption compared with the minimum-fuel maximum–minimum–maximum solution.

Feedback Gain Design

In the past applications of the DOC methodology, user-prescribed constant gains are used. For example, $K = -1$ is used in [21] for the vertical rocket landing problem. Good understanding of the problem is required in order to pick constant gains that work well, and at times, one set of constant gains does not work well for the entire domain upon which the problem is defined. Treating control gains as additional decision variables increases the dimension of search space of the optimization problem, and in the meantime, it lacks a direct way to manipulate the transients of the perturbed trajectories. In this section, a new way of prescribing control gains within the DOC framework is presented, using the discrete LQR technique. The control gains herein are computed as the nominal trajectory is being optimized. Thus, these gains are adaptive to problem-specific parameters such as boundary conditions, etc., and with the LQR technique, one can balance the weights on the states and controls to manipulate the transients of the closed-loop trajectories [16].

Let the time period from t_0 to t_f be divided into N intervals with $N + 1$ nodes. Let $\delta\mathbf{x}_i$ and $\delta\mathbf{u}_i$ denote the state and control deviations from their nominal values $\mathbf{x}_i^*$ and $\mathbf{u}_i^*$ at node i (i.e., $\mathbf{x}_i = \mathbf{x}_i^* + \delta\mathbf{x}_i$, and $\mathbf{u}_i = \mathbf{u}_i^* + \delta\mathbf{u}_i$). Then the nonlinear equations of motion $\dot{\mathbf{x}} = f(\mathbf{x}, \mathbf{u}, t)$ can be discretized and linearized about the nominal trajectory to obtain the following discrete linear time-variant system:

$$\delta\mathbf{x}_{i+1} = A_i \delta\mathbf{x}_i + B_i \delta\mathbf{u}_i, \qquad i = 0, 1, \ldots, N-1 \tag{17}$$

where A_i and B_i are the system matrices of the linearized system. To find a neighboring control policy that minimizes the state deviations at t_f, the following quadratic performance index is used:

$$\mathcal{V}_0 = \min_{\delta\mathbf{u}_i, i=0,1,\ldots,N-1} \delta\mathbf{x}_N^T Q \delta\mathbf{x}_N + \sum_{i=0}^{N-1} \delta\mathbf{u}_i^T R_i \delta\mathbf{u}_i \tag{18}$$

where $Q \geq 0$ and $R_i > 0$ are weighting matrices.

Iterative dynamic programming [16] is employed to obtain the solution to the discrete linear quadratic optimal control problem given by Eqs. (17) and (18), resulting in the following algorithm. At any node $0 \leq i \leq N-1$, the minimizing control policy is given by

$$\delta\mathbf{u}_i = K_i \delta\mathbf{x}_i \tag{19}$$

where

$$K_i = -(R_i + B_i^T P_{i+1} B_i)^{-1} B_i^T P_{i+1} A_i \tag{20}$$

and P_{i+1} can be constructed by

$$P_i = (A_i + B_i K_i)^T P_{i+1} (A_i + B_i K_i) + K_i^T R_i K_i; \qquad P_N = Q \tag{21}$$

Details of the solution procedure can be found in [22], though therein the same technique is used to solve a problem with a slightly different performance index than Eq. (18).

Power Descent Example

This section presents an example of powered descent problem, focusing on the comparison between the no-DOC solution and DOC solutions with various sensitivity penalty factors. Numerical solutions to problems no-DOC and DOC are obtained using the direct collocation method [23] and the software package EZopt [24], which uses the large-scale sparse nonlinear program solver SNOPT [25] as its background engine. Problem DOC_1 serves as a temporary step in the transition from problem no-DOC to problem DOC, and thus the solutions to problem DOC_1 are not pursued here. After an optimal nominal trajectory is obtained, 1000 Monte Carlo simulations are performed to assess the achievable landing precision in the presence of perturbations. The throttle bounds are implemented within the simulations. That is, if the throttle u exceeds its bounds, then the control vector $\mathbf{u} = [u_x, u_y, u_h]^T$ is scaled to ensure that u is always within its bounds; that is,

$$u_{x,y,h} = \frac{u_{x,y,h}}{u} \cdot u_{\max}, \quad \text{if } u > u_{\max}$$
$$u_{x,y,h} = \frac{u_{x,y,h}}{u} \cdot u_{\min}, \quad \text{if } u < u_{\min} \tag{22}$$

The vehicle model is selected to be similar to those in other studies [14,15] and is representative of the MSL lander. It is assumed that the lander carries 400 kg of fuel at the hand-off, with a total wet mass of 1905 kg. Other parameters of the lander used in the simulations are as follows:

$$n = 6, \qquad \phi = 27 \text{ deg}, \qquad g = 3.7114 \text{ m/s}^2$$
$$g_0 = 9.80655 \text{ m/s}^2, \qquad T = 3100 \text{ N}, \qquad I_{\text{sp}} = 225 \text{ s}$$
$$u_{\min} = 0.3, \qquad u_{\max} = 0.8$$

Table 1 shows the prescribed boundary conditions that are adopted from [14], with the addition of an initial velocity at the $\hat{y}$ direction. The combination of $x_0 > 0$ and $v_{x0} > 0$ indicates that the lander initially is moving away from the landing site. The lander is also moving away from the landing site at 20 m/s in the $\hat{y}$ direction. Such choice of initial conditions is one of the bad scenarios, as extra fuel has to be expended to stop the lander from moving away before it can be guided toward the target.

The following perturbations are significant during the powered descent and thus are considered in the Monte Carlo simulations. At the hand-off, the lander is up to 300 m off the desired position horizontally, and the velocity mismatches are up to 4 m/s in all three directions. Another source of perturbation stems from the uncertainty of the thrust produced by the thrusters, which is assumed to be ±5% of the nominal maximum thrust. It is also assumed that the perturbations are uniformly distributed within their bounds.

Simulations with the No-DOC Solution

The nominal trajectory for problem no-DOC is obtained first. The optimal maximum–minimum–maximum throttle profile is shown in Fig. 1, and the fuel consumption of 291.1 kg is shown in Fig. 2. Next, Monte Carlo simulations are performed on the open-loop system without the feedback control. The final position error spread is shown in Fig. 3a, in which each dot represents a simulation run. Not surprisingly, in the presence of perturbations, the landing errors at the final time (as much as ±500 m in all three directions) are enormous and exceed the ranges required for a pinpoint landing.

A new set of Monte Carlo simulations are then performed with the feedback control law in Eqs. (19) and (7) implemented. The following weight matrices Q and R_i are used in the feedback controller design algorithm:

$$Q = \text{diag}\{\,1, \quad 1, \quad 1, \quad 100, \quad 100, \quad 100, \quad 1\,\}$$
$$R_i = 20 \cdot \left[\frac{100}{N}(i-1)\right]^{2/3} \cdot I_{3\times 3}, \qquad i = 0, 1, \ldots, N-1 \tag{23}$$

The choice of Q places more emphasis on the reduction of the final velocity errors than the position error. Since the controls at later nodes have more direct effect than those at earlier nodes on the state deviations at the final time, the algorithm tends to render controls with larger magnitude at later nodes. Thus, R_i is chosen to be monotonically increasing with node i to balance the magnitude of controls throughout the trajectory.

Out of the 1000 simulation runs, all but 55 cases result in control bound violations. This is due to the fact that the nominal control rides on the bounds at all times. The closed-loop throttle profiles for all simulation cases, along with the upper and lower throttle bounds, are plotted in Fig. 4, which shows how frequently and how much the closed-loop throttles exceed the prescribed bounds. Figure 3b shows that the final horizontal position is within 60 m from the target, and the vertical position at the final time can be as much as 100 m below the target. Apparently, the errors in the vertical channel are not acceptable for a pinpoint landing. These plots also reveal that the majority of the errors in all three directions are negative. This is due to the fact that the scaling of the throttles that are out of bounds significantly undercuts the control authority of the thrusters.

Table 1 Boundary conditions

	x, m	y, m	h, m	v_x, m/s	v_y, m/s	v_h, m/s
At $t = 0$	1900	0	3100	40	20	−50
At t_f	0	0	0	0	0	0

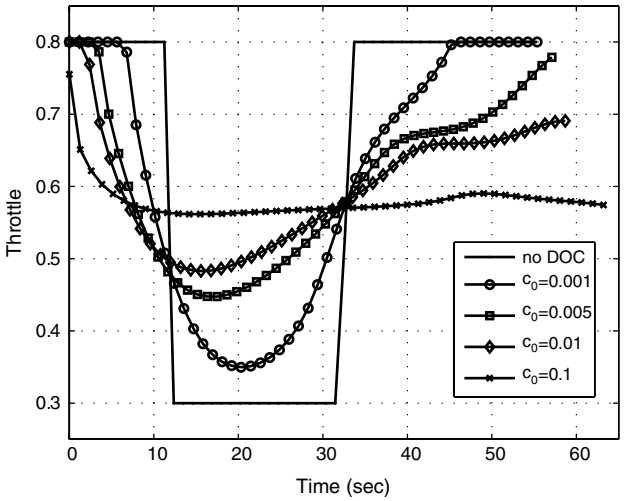

Fig. 1 Nominal throttle profiles.

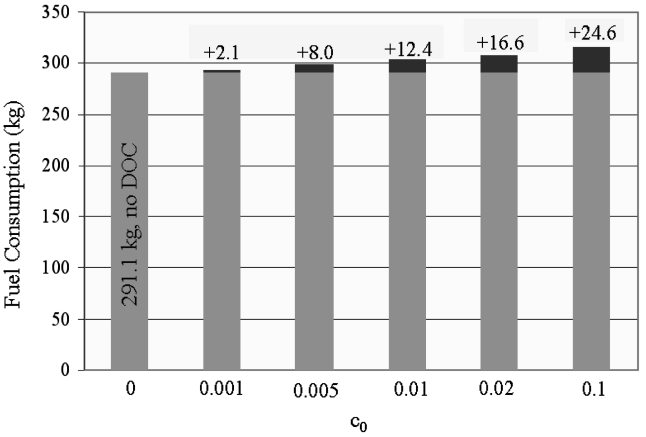

Fig. 2 Nominal fuel consumptions.

It should be pointed out that if the full magnitude of the feedback law is allowed (that is, without the scaling), the final position and velocity errors may be smaller, as intended by the LQR controller design. The fact that the simulations with the no-DOC solution do not show satisfactory results is not solely due to the feedback controller design, but also a consequence of the scaling of the closed-loop controls that exceed the thruster capacity. The next set of simulations will show how this situation can be alleviated by the DOC methodology and the multiplicative factor used to modulate the feedback control gains.

Simulations with the DOC Solutions

In this subsection, solutions to problem DOC for various penalty factors c_0 are obtained and compared to the no-DOC solution. As described in Eq. (10), weights c_i $(i = 1, \ldots, 6)$ can be chosen to leverage the emphasis on the sensitivity of each final position or velocity component with respect to state perturbations. This adds extra degrees of freedom in shaping the final landing errors. In this study, the following choice of c_i is used:

$$c_1 = c_2 = c_4 = c_5 = c_6 = 1; \qquad c_3 = 100$$

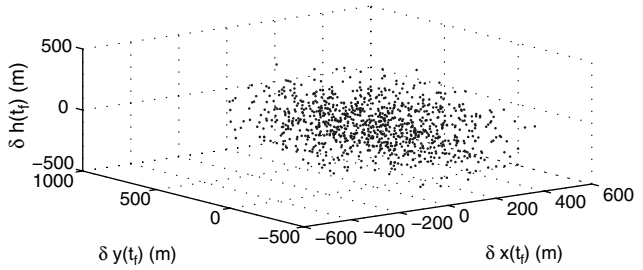

a) Without feedback

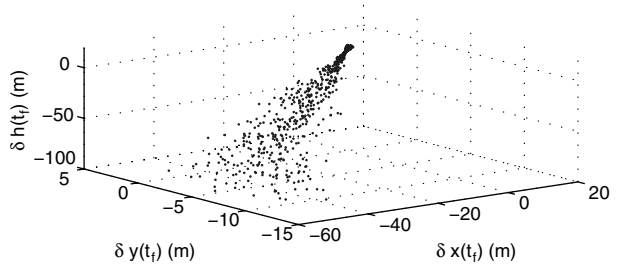

b) With feedback

Fig. 3 Final position error spread in the Monte Carlo simulations with the no-DOC solution.

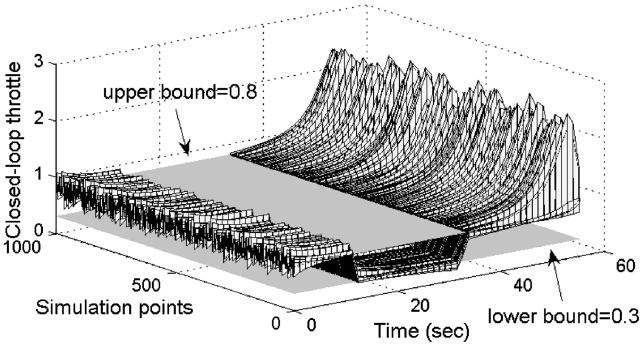

Fig. 4 Closed-loop throttle profiles in the Monte Carlo simulations with the no-DOC solution.

Since the vertical channel has less margin for errors than the horizontal channel, extra weight is placed on the vertical position sensitivity.

The nominal throttle profiles for problem DOC with various values of c_0 are shown in the same plot as the nominal no-DOC solution in Fig. 1. Compared to the no-DOC solution, the throttles for problem DOC no longer ride the prescribed bounds. In fact, as c_0 increases, the throttle seemingly approaches 0.55, which is halfway between the two bounds. As mentioned earlier, the nominal throttle approaching 0.55 may result in greater benefit in sensitivity reduction. However, it should be pointed out that one should not increase c_0 arbitrarily high, as the sensitivity reduction does not come free of adversaries. Intuitively, the further away the nominal solution is from the fuel-optimal maximum–minimum–maximum structure, the more fuel consumption it may incur. In fact, for a smaller c_0, an increase of its value can result in a great deal of sensitivity reduction with only a small amount of extra fuel consumption. As c_0 is increased to a certain level, the benefit of sensitivity reduction is far outweighed by the excessive extra fuel consumption.

The nominal fuel consumptions of the problem DOC solutions corresponding to various values of c_0 are shown alongside that of the no-DOC solution in Fig. 2, and the differences are clearly indicated. It can be seen that when $c_0 \leq 0.01$, the extra fuel consumption is less than 4.3% of that of the no-DOC solution. As c_0 is increased further, however, the extra fuel consumption may be deemed excessive and becomes difficult to justify in practice. For example, when $c_0 = 0.1$, an additional 24.6 kg of fuel is needed, constituting 8.45% of the consumption of the no-DOC solution. However, it will be shown next that no significant benefit in terms of reducing the final errors is gained by increasing c_0 from 0.01 to 0.1.

A set of Monte Carlo simulations are performed for each of the solutions with different c_0. The same choice of weight matrices are used in the controller design as in Eq. (23). The final errors when $c_0 = 0.001$ are in the same order of magnitude as that for the no-DOC solution shown in Fig. 3b, except that the positive and negative errors here are rather evenly distributed, which can be explained by the scarce occurrences of out-of-bound closed-loop controls. In fact, only 18 out 1000 simulations end up with throttles that are out of bounds. Even for those cases, the occurrences are limited to the first a few nodes, and the maximum throttle is below 0.86 (compared to the value of 3 in Fig. 4). Therefore, scaling the out-of-bound throttles does not significantly skew the distribution of the final errors.

As c_0 is increased, the final errors are reduced. When $c_0 = 0.005$, the final horizontal position errors are within 20 m, and the final altitude errors are within 12 m, significantly improved over the case when $c_0 = 0.001$. Further improvement is achieved when $c_0 = 0.01$, with the final error spreads shown in Fig. 5. The position errors are controlled to be largely within 5 m, and the vertical velocity is largely within 0.5 m/s. When c_0 is increased from 0.01 to 0.1, the largest final altitude error reduces from 4 to 2.5 m, and the largest final vertical velocity error reduces from 0.5 to 0.4 m/s. Therefore, in practice, such a small gain in the final error reduction probably does not justify the additional 12.2 kg of fuel consumption.

The time histories of the closed-loop throttle of the 1000 Monte Carlo simulations for the case with $c_0 = 0.01$ is shown in Fig. 6. It can be seen that the closed-loop throttles stay within the prescribed bounds in the vast majority of the cases. Indeed, this observation is prevalent for all of the simulated cases with a nonzero

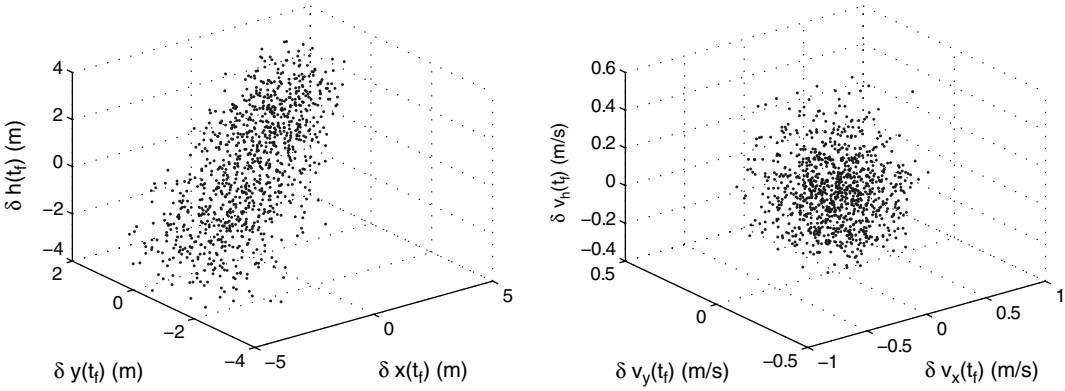

Fig. 5 Final error spreads in the Monte Carlo simulations with the DOC solution; $c_0 = 0.01$.

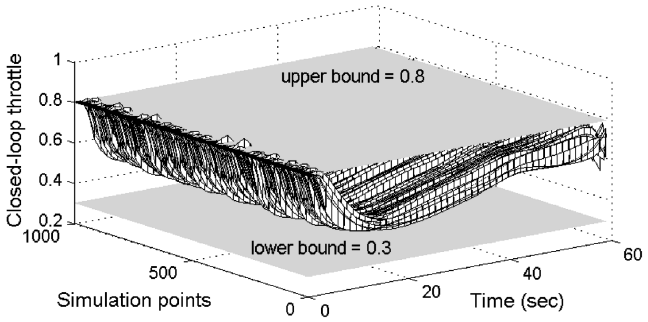

Fig. 6 Closed-loop throttle profiles in the Monte Carlo simulations with the DOC solution; $c_0 = 0.01$.

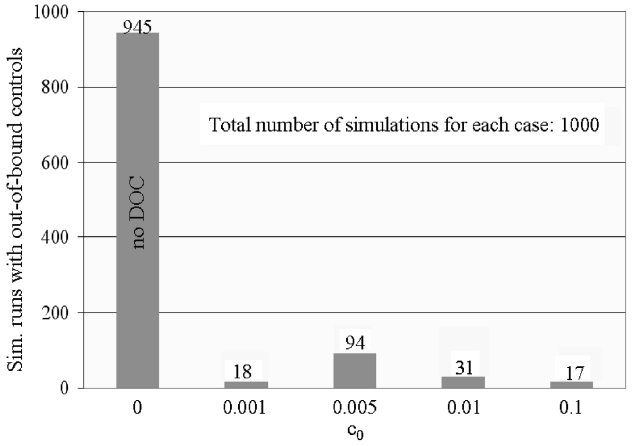

Fig. 7 Occurrences of simulation runs with out-of-bound closed-loop throttles in the Monte Carlo simulations.

c_0, as shown in Fig. 7, which summarizes the occurrences of simulation runs with out-of-bound throttles. It can be seen that the propensity of the out-of-bound closed-loop throttles is significantly reduced by applying the DOC methodology. Furthermore, during simulations with the DOC solutions, even in cases in which the upper bound is violated, the throttle magnitude remains below 0.86. Thus, no significant performance deterioration is caused by scaling the out-of-bound throttles. Finally, the spread of the fuel consumption is about ± 8 kg about the nominal values in all simulations.

Conclusions

This study clearly demonstrates the efficacy of the desensitized optimal control methodology to the problem of minimum-fuel powered descent on Mars, in the presence of uncertainties and perturbations. Within the desensitized optimal control framework, sensitivities of the final position and velocity with respect to state perturbations at all times are derived and augmented onto the minimum-fuel performance index through penalty factors. The linear quadratic regulator technique is used to design the feedback control gains. To reduce the likelihood of the closed-loop throttle exceeding the prescribed bounds, a multiplicative factor is applied to the feedback gains. The reshaping of the nominal trajectory from the well-known maximum–minimum–maximum profile due to the augmentation of the objective function and the multiplicative factor on the control gains is evident. Monte Carlo simulations with the reshaped desensitized nominal solutions show that the occurrences of out-of-bound closed-loop controls are significantly reduced compared to the simulations with the maximum–minimum–maximum solution, resulting in much improved landing precision. The improved landing precision is also achieved with little extra fuel consumption compared to the maximum–minimum–maximum solution. Monte Carlo simulations show that position errors of less than 5 m and velocity errors of less than 0.8 m/s can be achieved.

References

[1] Braun, R. D., and Manning, R. M., "Mars Exploration Entry, Descent and Landing Challenges," *Journal of Spacecraft and Rockets*, Vol. 44, No. 2, 2007, pp. 310–323. doi:10.2514/1.25116

[2] Braun, R. D., Powell, R. W., Cheatwood, F. M., Spencer, D. A., and Mase, R. A., "The Mars Surveyor 2001 Lander: A First Step Toward Precision Landing," 49th International Astronautical Congress, Melbourne, Australia, Paper IAF 98-Q.3.03, 1998.

[3] Wells, G. W., Lafleur, J. W., Verges, A. A., Manyapu, K. K., Christian, J. A., Lewis, C. A., and Braun, R. D., "Entry, Descent and Landing Challenges of Human Mars Exploration," *Advances in the Astronautical Sciences*, Vol. 125, American Astronautical Society, Springfield, VA, 2006, pp. 325–340; also 29th AAS Guidance and Control Conference, Breckenridge, CO. American Astronautical Society, Paper 06-072, Feb. 2006.

[4] Wolf, A. A., Graves, C., Powell, R. W., and Johnson, W., "Systems for Pinpoint Landing at Mars," *Advances in Astronautical Sciences*, Vol. 119, American Astronautical Society, Springfield, VA, 2005, pp. 2677–2696; also 14th AAS/AIAA Space Flight Mechanics Conference, Maui, HI, American Astronautical Society, Paper 04-272, Feb. 2004.

[5] Brand, T., Fuhrman, L., Geller, D., Hattis, P., Paschall, S., and Tao, Y. C., "GN&C Technology Needed to Achieve Pinpoint Landing Accuracy at Mars," AIAA/AAS Astrodynamics Specialist Conference and Exhibit, Providence, RI, AIAA Paper 2004-4748, Aug. 2004.

[6] Chu, C.-C., "Development of Advanced Entry, Descent, and Landing Technologies for Future Mars Missions," *IEEE Aerospace Conference*, Inst. of Electrical and Electronics Engineers, Piscataway, NJ, March 2006.

[7] Schmitz, P., Rebound, O., Ormston, T., and Mercolino, M., "Flight of the Phoenix: ESOC Supports NASA Mars Mission," *ESA Bulletin*, No. 134, May 2008.

[8] Carman, G. L., Ives, D. G., and Geller, D. K., "Apollo-Derived Mars Precision Lander Guidance," AIAA Atmospheric Flight Mechanics Conference, Boston, AIAA Paper 98-4570, Aug. 1998.

[9] Powell, R. W., "Numerical Roll Reversal Predictor-Corrector Aerocapture and Precision Landing Guidance Algorithms for the Mars Surveyor Program 2001 Missions," AIAA Atmospheric Flight Mechanics Conference, Boston, AIAA Paper 98-4574, Aug. 1998.

[10] Shen, H., Seywald, H., and Powell, R. W., "Desensitizing The Pin-Point Landing Trajectory on Mars," AIAA/AAS Astrodynamics Specialist Conference, Honolulu, HI, AIAA Paper 2008-6943, Aug. 2008.

[11] Lockwood, M. K., Powell, R. W., Graves, C. A., and Carman, G. L., "Entry System Design Considerations for Mars Landers," *Advances in the Astronautical Sciences*, Vol. 107, American Astronautical Society, Springfield, VA, 2001, pp. 311–346; also 24th Annual AAS Guidance and Control Conference, Breckenridge, CO, American Astronautical Society, Paper 01-023, 2001.

[12] Way, D. W., Powell, R. W., Chen, A., Steltzner, A. D., San Martin, A. M., Burkhart, P. D., and Mendeck, G. F., "Mars Science Laboratory: Entry, Descent, and Landing System Performance," *IEEE Aerospace Conference*, Inst. of Electrical and Electronics Engineers, Paper 1467, March 2007.

[13] Wong, E., Singh, G., and Masciarelli, J. P., "Guidance and Control Design for Hazard Avoidance and Safe Landing on Mars," *Journal of Spacecraft and Rockets*, Vol. 43, No. 2, 2006, pp. 374–384. doi:10.2514/1.19668

[14] Topcu, U., Casoliva, J., and Mease, K. D., "Minimum-Fuel Powered Descent for Mars Pinpoint Landing," *Journal of Spacecraft and Rockets*, Vol. 44, No. 2, 2007, pp. 324–331. doi:10.2514/1.25023

[15] Açikmeşe, B., and Ploen, S. R., "Convex Programming Approach to Powered Descent Guidance for Mars Landing," *Journal of Guidance, Control, and Dynamics*, Vol. 30, No. 5, 2007, pp. 1353–1366. doi:10.2514/1.27553

[16] Bryson, A. E., and Ho, Y. C., *Applied Optimal Control*, Hemisphere, New York, 1975, pp. 128–176.

[17] Seywald, H., and Kumar, R. R., "Desensitized Optimal Trajectories," *Advances in the Astronautical Sciences*, Vol. 93, 1996, pp. 103–116; also AIAA/AAS Space Flight Mechanics Conference, Austin, TX. American Astronautical Society, Paper 96-107, Feb. 1996.

[18] Zhou, K., Doyle, J., and Glover, K., *Robust and Optimal Control*, Prentice–Hall, New York, 1995.

[19] Charnes, A., and Cooper, W. W., "Chance-Constrained Programming," *Management Science*, Vol. 6, No. 1, 1959, pp. 73–79. doi:10.1287/mnsc.6.1.73

[20] Schwarm, A. T., and Nikolaou, M., "Chance-Constrained Model

Predictive Control," *AIChE Journal*, Vol. 45, No. 8, 1999, pp. 1743–1752.
doi:10.1002/aic.690450811

[21] Seywald, H., "Desensitized Optimal Trajectories With Control Constraints," *Advances in the Astronautical Sciences*, Vol. 114, 2003, pp. 737–744; also Space Flight Mechanics Conference, Ponce, Puerto Rico, American Astronautical Society, Paper 03-147, Feb. 2003.

[22] Driessen, B., and Sadegh, N., "Minimum-Time Trajectory Tracking of an Underactuated System," *Proceedings of the American Control Conference*, Vol. 4, Inst. of Electrical and Electronics Engineers, Piscataway, NJ, June 2000, pp. 2834–2838.

[23] Hargraves, C. R., and Paris, S. W., "Direct Trajectory Optimization Using Nonlinear Programming and Collocation," *Journal of Guidance, Control, and Dynamics*, Vol. 10, No. 4, 1987, pp. 338–342.
doi:10.2514/3.20223

[24] EZopt, Software Package, Analytical Mechanics Associates, Inc., Hampton, VA, 1997.

[25] SNOPT, Software Package, Ver. 7: Stanford Univ., Stanford, CA, Feb. 2006.